PCCP

Accepted Manuscript

ROYAL SOCIETY OF CHEMISTRY

www.rsc.org/pccp

High-throughput screening of high-capacity electrodes for hybrid Li-ion/Li-O_2 cells

S. Kirklin,[†] M. K. Y. Chan,[‡] L. Trahey,[¶] M. M. Thackeray,[¶] and C. Wolverton[*†]

†Department of Materials Science and Engineering, Northwestern University, Evanston, IL 60208, USA

‡Center for Nanoscale Materials, Argonne National Laboratory, Argonne, IL 60439, USA

¶Chemical Sciences and Engineering Division, Argonne National Laboratory, Argonne, IL 60439, USA

*To whom correspondence should be addressed. E-mail: c-wolverton@northwestern.edu

Abstract

Recent experiments have shown that lithium and oxygen can be electrochemically removed from Li_5FeO_4 ($5Li_2O{\cdot}Fe_2O_3$) and re-accommodated during discharge, creating the possibility of its use as a high-capacity electrode in a hybrid Li-ion/Li-O_2 electrochemical cell. Taking this novel chemistry as a model, we use density functional theory (DFT) within a high-throughput framework to screen for analogous reactions in other materials. We search for candidate materials possessing high capacity, voltages compatible with existing electrolytes, and reasonable electrical conductivity. We identify several promising candidate materials that may operate by a similar reaction mechanism and are worthy of investigation, such as Li_6MnO_4, Li_6CoO_4, Li_4MoO_5 and Li_8IrO_6. This work paves the way for accelerated exploration of this intriguing new battery chemistry.

1. Introduction

The current state-of-the-art device for practical, dense and lightweight electrochemical energy storage is the lithium-ion battery (LIB). Since the commercialization of Li-ion batteries by Sony Corporation in 1991, no other battery chemistry has been able to match their combined energy density, cycle life and power density characteristics. Looking to

the future, the biggest impediment to further improvement of LIBs is the capacity limitation of current cathode materials, i.e., the extent to which they can tolerate lithium insertion/extraction reactions.[1] Cyclic stability of these reactions often requires that the host lattice retain its structure on lithiation and delithiation, which places a limitation on the amount of lithium that can be stored. Even the highest capacity LIB cathode materials provide only a few hundred mAh/g capacity, typically 150-200 mAh/g.[1]

In order to go beyond these limits, alternative battery chemistries such as Li-O_2 are being explored.[2,3] The theoretical oxygen electrode capacity of this electrochemical couple is 1795 mAh/g, when based on the mass of the fully discharged product (Li_2O), or 1169 mAh/g, when based on the conventional, partially discharged product (Li_2O_2). In spite of such staggering theoretical capacities, there are several significant and challenging technological hurdles that must be overcome before viable Li-O_2 cells are produced. Several excellent reviews have been written that highlight the challenges and opportunities of Li-O_2 batteries.[4–10] One of the most significant barriers to Li-O_2 cell operation is catalytic inefficiency at the cathode. Low power density, high charging over-potentials, and poor cycle life have all been attributed to the poor performance of the oxygen electrode.[11] In order to overcome these challenges, it is appealing to consider alternative concepts and approaches to exploit Li-O_2 electrochemistry.

Trahey *et. al.* have shown that Li_5FeO_4[12] and Li_2MnO_3[13] can be electrochemically delithiated at high potentials, and subsequently discharged, ultimately recovering their initial composition. In particular, they discovered that, after charging a Li_5FeO_4 electrode between 3.7 and 4.6 V in a Li/Li_5FeO_4-O_2 cell, the subsequent discharge between 3.2 and 2.9 V generated the same capacity as the initial charge (475 mAh/g), before reaching the 2.7-2.6 V plateau, which is the typical measured voltage of the discharge reaction in conventional Li-O_2 cells. Compared to the Li-O_2 reaction without Li_5FeO_4 in the same setup, the overpotential

for the reaction involving Li_5FeO_4 is reduced by 0.8 V, which leads to a substantial improvement in round-trip energy conversion efficiency.[12] The experimental data and supporting theoretical calculations[14] suggest that the reaction between 3.2 and 2.9 V proceeds predominantly by the addition/removal of Li and O_2 in the stoichiometric ratio Li:O = 2:1, as shown in reaction 1.

$$Li_5FeO_4\,(5Li_2O{\cdot}Fe_2O_3) \leftrightarrow 4Li + O_2 + LiFeO_2\,(Li_2O{\cdot}Fe_2O_3). \quad (1)$$

It should be noted that crystalline Li_2O is not formed during the reaction. Studying highly lithium-rich metal oxide materials, such as Li_5FeO_4, can be challenging because they are extremely moisture sensitive. As a result, great care must be taken to prepare and characterize these materials. Experimental screening of a large number of materials can therefore be a challenging and arduous task. Significant time and effort can be saved by using computational techniques to predict and guide the selection of promising materials for experimental evaluation. To accelerate the search for reaction chemistries similar to that shown by Li_5FeO_4, we have investigated thermodynamic equilibrium reaction paths for a wide range of lithium-rich metal oxide compounds using density functional theory (DFT).

In order to validate DFT as a method to evaluate the reaction of metal oxide electrodes with lithium and oxygen, we compare the DFT-predicted voltage profile of a Li/Li_5FeO_4–O_2 cell with the experimental voltage profile, as shown in Figure 1. Experimentally, almost three lithium ions and a corresponding amount of oxygen are extracted from Li_5FeO_4 in a Li/Li_5FeO_4-O_2 cell between 3.7 and 3.9 V before the cell voltage rises rapidly to about 4.5 V at which further lithium and oxygen are evolved, likely with simultaneous oxidation of the electrolyte.[12] On the subsequent discharge, all this capacity can be recovered between 3.2 and 2.9 V, which is higher than the electrochemical potential expected for Li_2O_2 formation (~2.6-2.7 V). Note that Johnson et al.[15] have reported that exactly four lithium ions can be extracted at a very slow rate from Li_5FeO_4 ($Li_2O{\cdot}Fe_2O_3$)

below 4 V in a Li/Li_5FeO_4 coin cell (i.e., in the absence of oxygen), corresponding to the removal of two Li_2O units and the generation of the rocksalt composition ($Li_2O{\cdot}Fe_2O_3$, or simply $LiFeO_2$), before the rapid increase in cell voltage occurs. Experimentally, there is a high overpotential during the charge reaction, which makes it difficult to remove the remaining lithium and oxygen from the '$LiFeO_2$' product without the interference of electrolyte decomposition. Nevertheless, the DFT calculations reproduce the presumed discharge voltage to within ~200 mV and they appear to correctly predict that further lithium and oxygen removal from the $LiFeO_2$ composition would occur at about 600 mV higher than the extraction of Li_2O from Li_5FeO_4 to generate first $LiFe_5O_8$ ($0.5Li_2O{\cdot}2.5Fe_2O_3$) before the iron oxide end-member, Fe_2O_3, is produced.[14] The discrepancy between the experimental and theoretical charging potentials is attributed to the high polarization that can occur at the oxygen electrode of Li-O_2 cells. The discrepancy in total capacity may be attributed to the difficulties in determining the amount of unreacted electrode material at the beginning of the charge reaction.

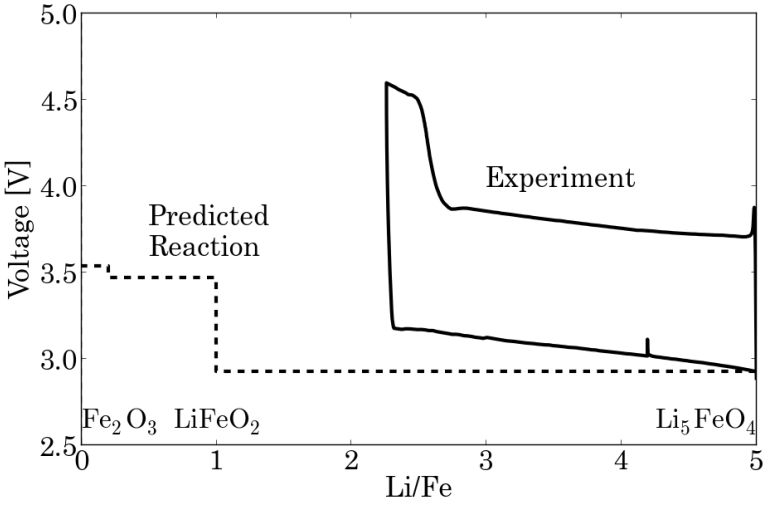

Figure 1. Comparison between DFT predicted reaction voltage (dashed line) and experimental charge/discharge profiles (solid line)[12]

In order to search for analogous reactions to that observed in Li_5FeO_4, the key characteristics of the reaction must first be defined. We begin by constructing a generalized

reaction for reaction 1:

$$(Li_2O)_n\cdot(A_xO_y) \leftrightarrow m(2Li + \tfrac{1}{2}O_{2(g)}) + (Li_2O)_{n-m}\cdot(A_xO_y) \quad (2)$$

For the model case, Li_5FeO_4, A_xO_y is Fe_2O_3 (A=Fe, x=2; y=3) and n=5. The reaction is written such that m corresponds to the number of Li_2O units that are removed (as lithium and oxygen) from the parent structure. Eq. 2 emphasizes the key characteristic of the reaction, which is the removal and re-accommodation of Li_2O units during charge and discharge, respectively, when the iron ions in the residual metal oxide structure would ideally maintain a constant trivalent state. In practice, however, we believe that the charge/discharge processes in Li_5FeO_4 electrodes are accompanied, at least partially, by the oxidation/reduction of some iron ions that may help catalyze the reactions between lithium and oxygen;[14] such redox reactions would contribute (at least marginally) to the capacity of 'hybrid' Li-O_2/Li-ion electrode materials containing transition metal ions. These redox reactions are beyond the scope of our screening process. Using the notation of reaction 2, a search through tens of thousands of known crystalline compounds was then conducted to identify other materials that may operate electrochemically by a mechanism of lithium and oxygen removal and re-accommodation (net loss/gain = Li_2O).

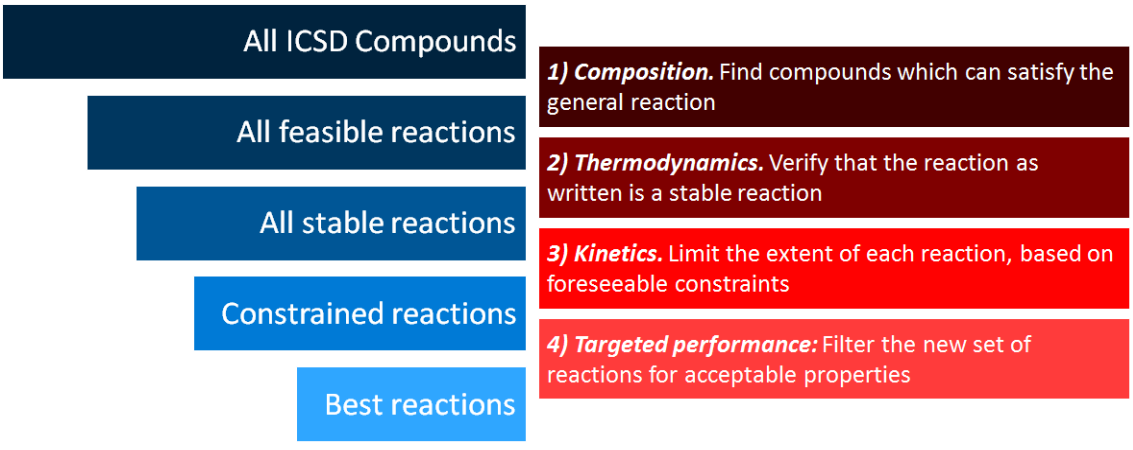

Figure 2. The four steps of the screening process used in this study.

A 4-step screening strategy (shown schematically in Figure 2) was employed to search for compounds with suitable composition, thermodynamic and kinetic properties.

Beginning with a pool of all compounds in the Inorganic Crystal Structure Database (ICSD),[16] the following sequential process was used to filter out the reactions that are most likely to be of potential interest for hybrid Li-ion/Li-O_2 cells:

- **Composition:** Identify materials which can satisfy reaction 2, *i.e.* all $Li_{2n}A_xO_{y+n}$ compounds for which a compound A_xO_y also exists in the ICSD.
- **Thermodynamics:** Remove reactions where the ground state reaction pathway differs from reaction 2. The ground state reaction pathway was determined using grand canonical linear programming (GCLP) and the Open Quantum Materials Database (OQMD).[17–19]
- **Kinetics:** Apply constraints to the reactions, which differ from the screening method used to remove reactions from the pool of candidates, by imposing limits on the reactions based on reasonable kinetic barriers and experimental conditions.
- **Targeted performance:** Finally, screen the constrained reactions based on a set of target performance metrics such as capacity and band gap values.

The results of this materials screening process are discussed in this paper. Candidate systems are specified that are worthy of experimental evaluation. Similar high throughput screening strategies have shown success previously in Li-ion battery electrode discovery,[20–23] it provides a rapid and effective method to focus experimental studies on those systems which may lead to the discovery of new high-performing electrode materials.

2. Methods

2.1 Density Functional Theory

All DFT[24,25] calculations were performed with the Vienna *Ab Initio* Software Package (VASP)[26–29] using projector augmented wave potentials.[30] For the systems considered in Thackeray *et. al.*[14] (Li_5FeO_4, Li_6CoO_4, Li_6MnO_4), plane wave cutoffs of 400 eV and 520 eV were tested for structural relaxation and the resulting volume differences were found to be

less than ~3%, so all further structural relaxations were performed at 400 eV. The Generalized Gradient Approximation (GGA) was used for the exchange-correlation functional as parameterized by Perdew, Burke and Enzerhoff (PBE).[31,32] The k-point mesh was constructed such that $N_{atoms} * N_{kpts} \approx 8000$ in a Γ–centered mesh. Any species with a partially filled *d*-shell was given an initial magnetic moment of 5 μ_b in a ferromagnetic structure.

For transition metal (Cr, Mn, Fe, Co, Ni, Cu) oxides, DFT+U was applied using U-values fitted to reproduce experimental oxidation energies as found by Wang *et. al.*[33] For all species with non-solid standard reference states (O_2, N_2, F_2, Cl_2, Br, and Hg), because the DFT ground state is not representative of the energy of the reference state, chemical potentials were fitted[34] to experimental data from the SGTE Substances database (SSUB).[35]

Further corrections were added to the elemental reference energies of all species which have DFT+U applied, using the fitted elemental-phase reference energies[36] (FERE). In this method, chemical potentials were determined by a simple least squares fit to experimentally measured formation energies. All calculations performed for this work are included in the Open Quantum Materials Database (OQMD).[19]

2.2 First Screen - Composition

The four-step screening strategy (Figure 2) was initiated by identifying Li_2O-containing compounds which, upon Li_2O removal, arrive at phases that satisfy reaction 2. Starting from the set of all compounds in the ICSD, we found all compounds $Li_{2n}A_xO_{y+n}$ such that a compound at A_xO_y also exists in the ICSD. This search process therefore identifies all compounds that can be represented as a linear combination of Li_2O and an oxide, A_xO_y. The placeholder 'A' in this formula is allowed to take on any value, including any linear combination of elements (including Li). From this search, we found 255 unique A_xO_y compounds that satisfy this criterion. Note that for some compounds, DFT calculations were

not performed due to partially-occupied sites or incomplete information.

2.3 Second screen - Thermodynamics

After identifying compounds that can satisfy lithium and oxygen (Li_2O) removal, i.e., reaction 2, this list of compounds was screened on the basis of a thermodynamically stable reaction path. The reaction path is dictated by the ground state convex hulls, which were determined using the quickhull algorithm[37] as implemented in qhull. If the ground state reaction path did not follow the form of reaction 2, the reaction was rejected. For example, $LiNaSO_4$ (alternatively, $Li_2O{\cdot}Na_2S_2O_7$) and $Na_2S_2O_7$ are compounds that are listed in the ICSD. However, DFT calculations showed that $LiNaSO_4$ is unstable relative to a two-phase Li_2SO_4 + Na_2SO_4 product, and is therefore not compliant with reaction 2; $LiNaSO_4$ was therefore discarded from the screen.

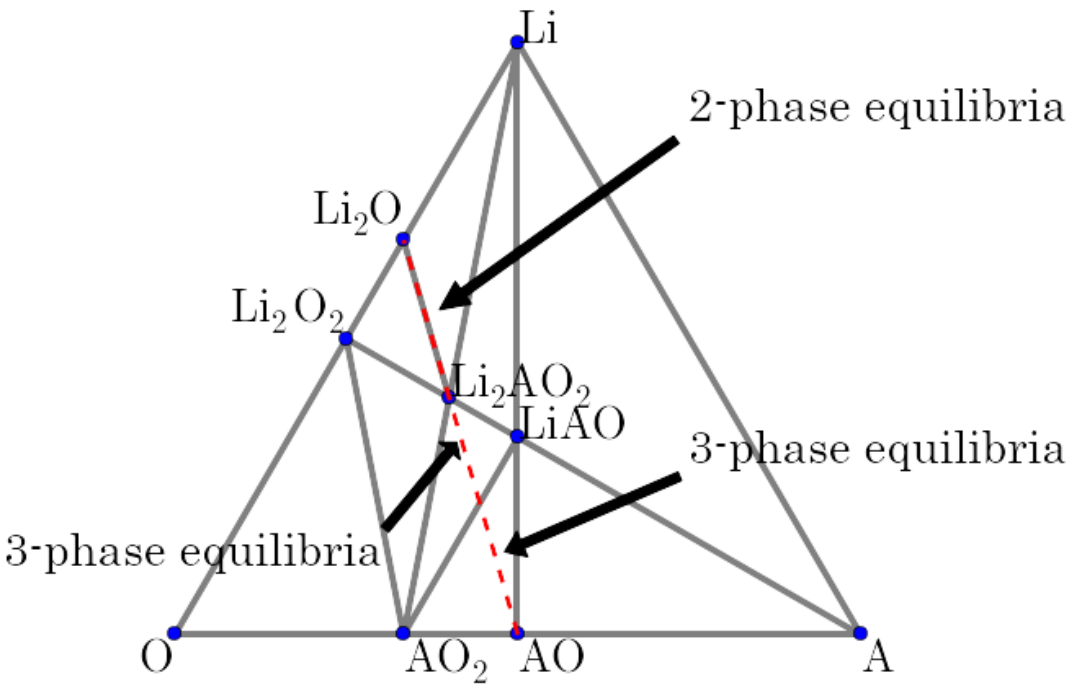

Figure 3. Schematic illustration of a Li-A-O phase diagram.

Reactions that do not occur via a two-phase reaction are also excluded. This criterion is based on our hypothesis that any reaction that requires the formation of multiple phases will have significantly higher requirements for mass transport and will be less likely to

accommodate facile, reversible phase separation and recombination. This problem was circumvented by selecting only reactions which follow exactly the form of reaction 2; i.e., reactions that occur along discrete tie-lines. An example of a reaction which does not exist in two-phase equilibria is shown by the dotted line in Figure 3. While there are many quaternary and higher order compounds that meet the composition requirement, this criterion eliminates all such reactions from consideration. This screen results in a pool of 55 systems with stable Li/O removal reactions.

2.4 Third Screen – Kinetics

In addition to electrode thermodynamics, additional constraints based on battery operation, namely electrolyte stability and electronic transport, can be imposed. First, in a battery, the reaction can be terminated once the voltage reaches a predefined threshold, thereby limiting the practical capacity. Second, if the intrinsic electronic conductivity of a product phase is too low, the rate at which the reaction proceeds will be impeded. These operating constraints can be applied as the following screens to our pool of reactions: 1) From our database of computed reactions, a maximum allowed reaction voltage was applied; 2) To screen for electrical conductivity, it was assumed that the conductivity decreases as the band gap increases, and therefore, screens were applied by setting a maximum allowed band gap on both products and reactants of each reaction. Figure 4 illustrates these screens for the Li_5FeO_4 reaction by setting a voltage cutoff of 3.5 V and a band gap cutoff of 4 eV. For the extraction of Li_2O from Li_5FeO_4 ($5Li_2O{\cdot}Fe_2O_3$) to Fe_2O_3, a voltage cut off of 3.5 V cuts off the last 2 steps in the reaction (to $LiFe_5O_8$ and Fe_2O_3). The band gap cutoff of 4 V only excludes Li_2O, which is not expected anyway. Constraining the reactions in this way should improve the ability to predict the accessible capacity. In the next section, we explain how these properties are computed, and how they are applied as selection criteria. It should be noted that the subsequent criteria (voltage and band gap) can be applied within a flexible

range of values to yield different sets of results. Two such sets – one with more stringent requirements than the other, but both with the same target capacity metric of 500 mAh/g – will be presented.

2.5 Voltage Cutoff Selection

The cell voltage for each reaction step is given by

$$V = \frac{\Delta G_f}{2F\Delta N_{Li_2O}} \tag{3}$$

where F is the Faraday constant, ΔG_f is the (molar) change in free energy of the reaction and ΔN_{Li2O} is the amount of Li_2O removed/added. The voltage is proportional to the derivative of the free energy along the reaction direction. At 0 K, the free energy surface has no curvature, so the derivative reduces to the change in energy across the reaction, divided by the change in amount of Li_2O. The factor of two in Eq. 3 comes from the fact that each Li_2O unit carries two electrons.

In this work, the change in free energy was approximated by neglecting the change in entropy of the solid phases, and only considering the change in entropy associated with the evolution of O_2 gas at standard temperature and pressure. Note that lithium and oxygen are assumed to be in their reference states of metallic Li and gaseous O_2. Eq. 3 was used to compute voltages for every reaction step, and a cutoff filter applied to exclude reactions above a threshold voltage based on the stability of available electrolytes. This cutoff must be greater than 2.8 V, because that is the voltage at which Li_2O is formed from the most highly-rich Li_2O phase and, therefore, is the lowest voltage step in every reaction path.

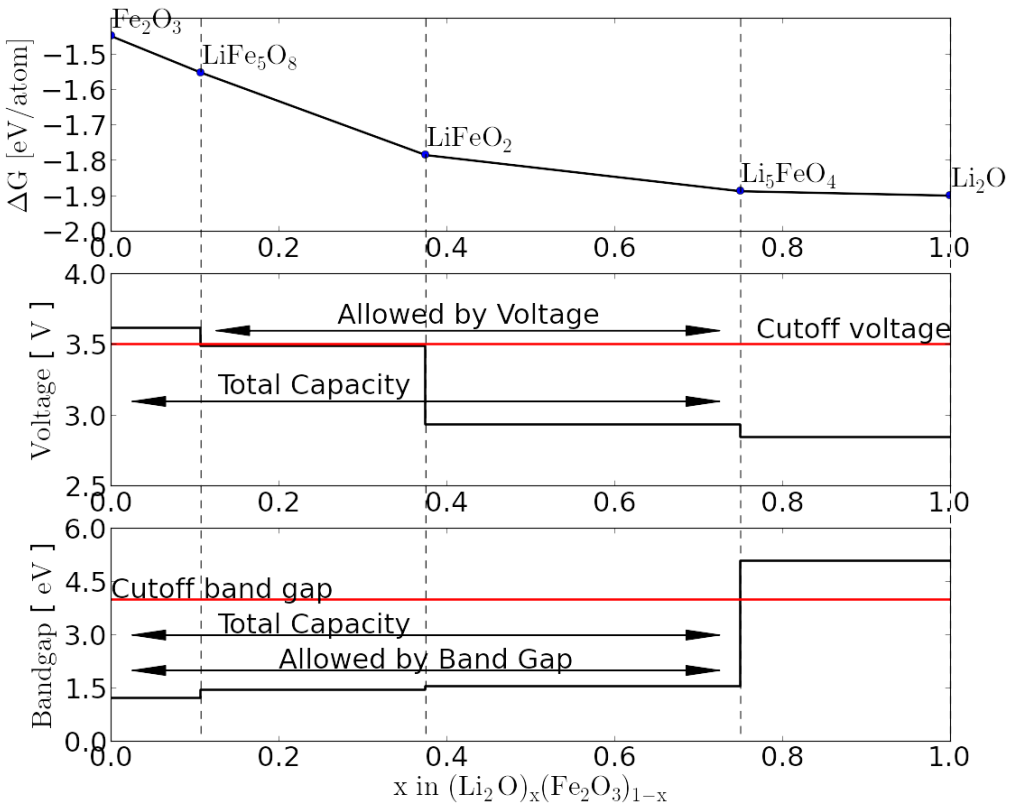

Figure 4. (top) Convex hull along the composition line connecting Fe_2O_3 to Li_2O; (middle) cell voltage as a function of this reaction coordinate; and (bottom) the widest band gap of any phase present as a function of reaction coordinate. On these plots, the effects of assigning a cutoff voltage of 3.5 V and a band gap of 4 eV are illustrated. Cutoffs are indicated by red lines, while the blue arrows indicate which reactions pass the screen.

The selection of the upper voltage threshold was based on the stability of current electrolyte solvents, which is significantly compromised if the charging voltage reaches 4.5 V because of oxidation and possible side reactions.[38,39] If it is assumed that there is an overpotential of at least 0.5 V[40] when charging these materials, the cutoff threshold should be set at 4 V.

2.6 Band Gap Cutoff Selection

Assuming only intrinsic carrier populations, materials with very wide band gaps are expected to have extremely low electronic conductivity, while those with smaller band gaps should have higher electronic conductivity. For this reason, the DFT Kohn-Sham band gap (i.e. eigenvalue gap)[41–43] was used as a surrogate for monitoring the electrical conductivity.

While the Kohn-Sham band gap from local or semi-local exchange-correlation functionals (such as PBE, which is used here) is systematically lower than the observed band gap,[44] it serves to indicate broad trends in the true band gaps. As an example, Figure 4 shows the calculated band gap as a function of Li_2O content for Li_5FeO_4. A reaction is screened by the widest band gap of all compounds involved in the reaction. The widest gap is chosen as a descriptor because the least conducting phase involved in the reaction represents a possible bottleneck to system performance. In general, the band gap is wider for compounds with higher Li_2O content. Because the conductivity is not limited to the intrinsic carrier concentrations, and is not a simple function of band gap only, we present two screens: one which tightly constrains band gap and one which does not.

2.7 Final screen - Targets

Once the final set of reactions has been determined, the list was reduced to sets of continuous reactions. For example, the Li_5FeO_4 to $LiFeO_2$ reaction passes all filters, as does the $LiFeO_2$ to $LiFe_5O_8$ reaction. These two reactions yield a combined Li_5FeO_4 to $LiFe_5O_8$ reaction. The gravimetric and volumetric capacity and energy corresponding to the resulting set of reactions were then computed according to the following equations:

$$C_{\mathrm{g}}(V) = \frac{n(V)F}{m_{Li_{2n}A_xO_{y+n}}} \tag{4}$$

$$C_{\mathrm{v}}(V) = \frac{n(V)F}{v_{Li_{2n}A_xO_{y+n}}} \tag{5}$$

$$E_{\mathrm{g}}(V) = \int_{V_{Li_2O}}^{V'} C_g(V')dV' \tag{6}$$

$$\mathrm{E_v(V)} = \int_{\mathrm{V_{Li_2O}}}^{\mathrm{V'}} \mathrm{C_V(V')dV'} \tag{7}$$

The total charge transferred at a specified voltage, (*n(V)* in Eqs. 4-7) was determined by the voltage profile of the reaction, multiplied by Faraday's constant times twice the

number of Li_2O released (for the $2e^-$ per Li_2O). The charge was then normalized by mass or volume to obtain the gravimetric (C_g) or volumetric (C_v) capacities, respectively (Eqs. 4 and 5). The phase with the highest mass or volume in the reaction was always used, so that the computed capacity was representative of the maximum electrode weight or volume. By integrating the gravimetric capacity as a function of voltage, the specific energy (E_g), was determined (Eq. 6). Similarly, by integrating the volumetric capacity as a function voltage, the energy density (E_v) was calculated (Eq. 7). (Note that because voltage and volume are both traditionally abbreviated as V, we use V to refer to voltage, and v to refer to volume.) Finally, when integrating over the potential-capacity curve, the lower limit of the integral, V_{Li2O}, is the voltage of the reaction $4Li + O_2 \rightarrow 2Li_2O$. The gravimetric capacity was used as a final filter. This final screen was implemented by sorting all reactions by gravimetric capacity and selecting the highest capacity reactions.

3. Results

All 255 materials and reactions which pass the first screen (composition) are shown in Figure 5. Figure 5(a) shows a plot of initial voltage (corresponding to the reaction step involving compounds with the lowest lithium contents) vs. gravimetric capacity, with marker colors indicating the largest band gap in the reaction path, and the marker shape indicating whether or not the reaction passes the second screen (thermodynamics). Circular markers are reactions which pass the second screen, while X markers are those which fail on the second screen. Figure 5(b) is a plot of specific energy vs. energy density. In both plots, the position of the Li_5FeO_4 reaction is highlighted. In addition, in Figure 5(a) and Figure 5(b) the position of the standard Li-ion reaction, $2LiCoO_2 + C_6 \leftrightarrow 2Li_{0.5}CoO_2 + LiC_6$, and the position of the reaction for the removal of Li_2O from Li_2MnO_3 are also indicated for comparison. The highest onset voltage for the reactions of the initial screen of 255 compounds was approximately 5.0 V. The lower bound on all reaction voltages is 2.8 V, which is the

computed reaction voltage for Li_2O formation; it is the voltage of the last step of every computed reaction, because the last step always reflects the equilibrium reaction between the closest Li_2O-rich phase and Li_2O.

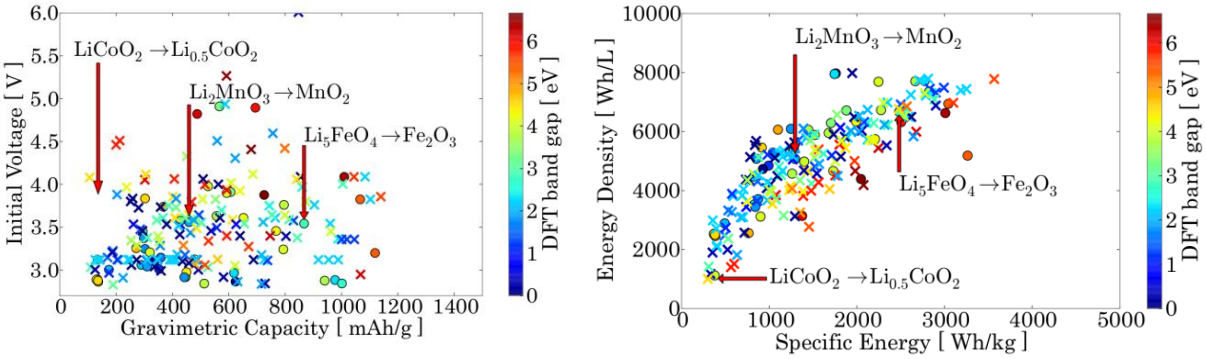

(a) Voltage vs. capacity with band gap

(b) Specific energy vs. energy density with band gap

Figure 5. Summary of Li_2O addition/removal reactions found by this study. All filters are subsequently applied to this initial set of reactions. (Left) Plot of gravimetric capacity vs initial voltage. The color of each marker indicates the widest band gap of any step of the reaction, with red indicating wide band gap reactions and blue indicating narrow band gap reactions. The shape of the marker indicates whether reaction 2 is thermodynamically stable (circles are stable, crosses are unstable and reflect rejected reactions). (Right) Plot of specific energy vs. energy density.

From this preliminary screen, it is clear that Li_5FeO_4 appears to be one of the best prospects in this class of materials. However, the screen exposed other reactions that offer as good or better capacity than Li_5FeO_4, several of which are strongly suggested for future experimental investigation.

3.1 Predictions – most restrictive constraints

We find eight materials and reactions that meet all of the screening criteria described above, i.e., they are stable compounds; they operate by 2-phase reactions that do not exceed 4 V; and the band gap is less than 4 eV. These materials and reactions are indicated by arrows in Figure 6. The reaction for Li_5FeO_4, which provides the motivation for this work, is identified by a red arrow. For these eight reactions, the full reaction path, as well as a complete description of voltages, capacities and band gaps, is provided in Table 1.

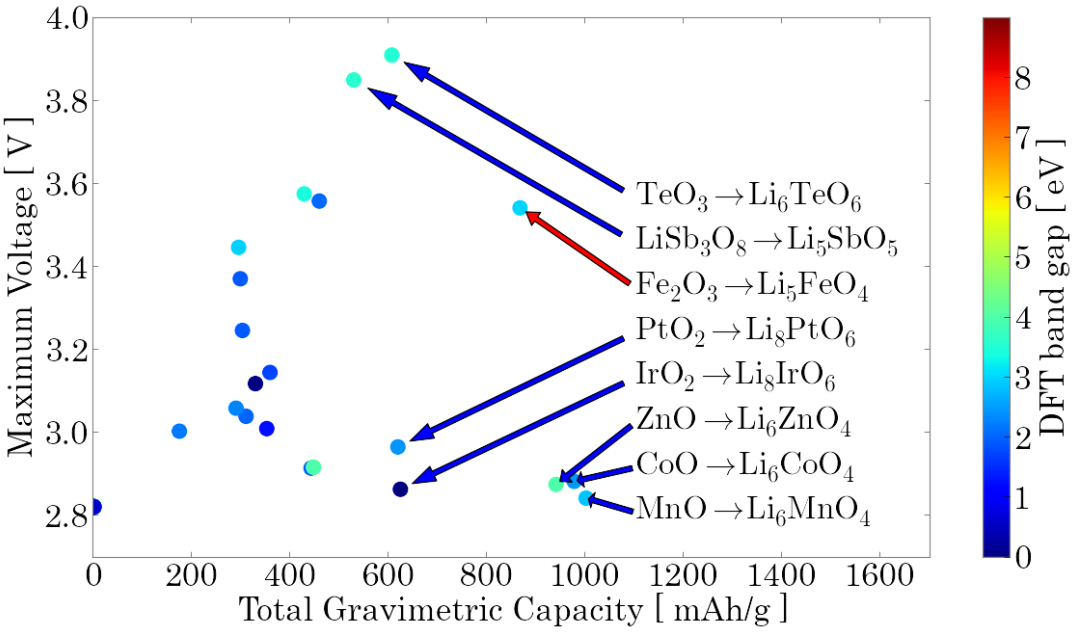

Figure 6. Results of restrictive screening, highlighting reactions that provide a capacity >500 mAh/g below 4 V, with every phase having a DFT band gap below 4 eV. For systems involving several reaction steps such as the Li_5FeO_4 example in Figure 4, the maximum voltage is reported.

Table 1. Full reaction pathway for each reaction which passes the restrictive screens. For each step the product phases, voltages, gravimetric and volumetric capacities, energy densities and specific energies are reported.

Reaction steps	Voltage [V]	C_g [mAh/g]	C_V [mAh/mL]	E_g [Wh/kg]	E_V [Wh/L]	Band gap [eV]
Li_5FeO_4						
→ $LiFeO_2$	2.9	694	1864	1958	5259	3.0
→ $LiFe_5O_8$	3.5	832	2237	2362	6346	1.5
→ Fe_2O_3	3.6	867	2330	2483	6670	1.5
Li_6CoO_4						
→ $Li_{10}Co_4O_9$	2.9	570	1585	1609	4475	2.5
→ CoO	2.9	977	2718	2773	7714	1.4
Li_6MnO_4						
→ MnO	2.8	1001	2609	2826	7364	2.9
Li_6ZnO_4						
→ $Li_{10}Zn_4O_9$	2.9	548	1585	1548	4472	4.0
→ ZnO	2.9	940	2717	2667	7706	2.6
Li_8IrO_6						
→ IrO_2	2.9	624	2825	1760	7972	0.0
Li_8PtO_6						
→ PtO_2	3.0	619	2916	1746	8230	2.4
Li_5SbO_5						
→ Li_3SbO_4	3.0	227	836	639	2361	3.4
→ $LiSbO_3$	3.3	454	1673	1310	4836	3.6
→ $LiSb_3O_8$	3.9	567	2091	1704	6290	2.5

Li_6TeO_6						
→	Li_4TeO_5	3.1	202	722	571	2035	3.5
→	Li_2TeO_4	3.4	404	1443	1188	4240	3.0
→	TeO_3	3.9	606	2164	1882	6715	2.7

The materials (and reactions) which pass all screens can be divided into three groups that can be distinguished from one another according to the metals in the oxides. There are four 3*d* transition metal oxides (**Li_5FeO_4**, **Li_6CoO_4**, **Li_6MnO_4**, and **Li_6ZnO_4**), two metalloid oxides (**Li_5SbO_5**, **Li_6TeO_6**), and two platinum group metal oxides (**Li_8PtO_6**, **Li_8IrO_6**).

Li_5FeO_4 is the compound that inspired this search. Its identification is a successful validation of our computational approach, the reaction metrics and reaction constraints in the screening process. Li_5FeO_4 has a defect anti-fluorite structure; it has been studied previously as a Li-ion battery cathode from which only about 0.5 Li per formula unit could be extracted.[45,46] Johnson et al. have demonstrated that 4 Li^+ ions, corresponding to 2 Li_2O units, can be extracted from Li_5FeO_4 at a slow rate, thereby significantly increasing the capacity of the electrode through oxygen release.[15] Three other 3*d* transition metal oxides, **Li_6CoO_4**, **Li_6MnO_4**, and **Li_6ZnO_4** (or $3Li_2O{\cdot}MO$, M = Co, Mn, Zn, respectively) with a defect anti-fluorite-type structure were identified in the search. In this case, the transition metals are divalent, and contain a higher Li_2O content than Li_5FeO_4, (in which the iron is trivalent), and offer slightly higher capacity. **Li_6CoO_4** has the smallest predicted band gap among the 3*d* transition metal oxide reactions, which may lead to superior electronic conductivity, and higher rate capabilities. **Li_6MnO_4** is distinct from the other 3*d* oxides, in that it is the only reaction that is predicted to decompose directly into the binary oxide. Both Li_6CoO_4 and Li_6MnO_4 have been investigated as Li-ion battery cathodes.[46] It was reported that 1 Li could be extracted from Li_6CoO_4 whereas, surprisingly, Li_6MnO_4 could not be delithiated. Li_6NiO_4 is conspicuous by its absence in Table 1. Because Li_6CoO_4 and Li_6MnO_4 are known compounds, DFT calculations were performed on a hypothetical Li_6NiO_4 anti-fluorite

structure to determine whether this phase should exist or not. It was found that Li_6NiO_4 in the anti-fluorite structure is unstable with respect to NiO and Li_2O, which is in agreement with the experimental observation that it does not form. The 3*d* transition metal oxide, **Li_6ZnO_4**, has been studied as a fast Li conductor.[47] Because **Li_6ZnO_4** has high Li mobility and offers high theoretical gravimetric and volumetric capacities (Table 1), it would therefore be of interest to determine the reaction kinetics of this material in a Li-O_2 cell. The ion conductivity of $Li_{5.5}Fe_{0.5}Zn_{0.5}O_4$ has also been found to be three orders of magnitude higher than that of Li_5FeO_4 at 100°C.[48] Therefore, the mixed-metal the Fe-Zn system may prove particularly attractive.

With respect to the platinum group metal oxides, **Li_8IrO_6 and Li_8PtO_6**, the reactions are predicted to provide capacities greater than 600 mAh/g, good electronic conductivity and a low charge/discharge voltage. Unfortunately, because these compounds contain rare and expensive elements, widespread use is unlikely. Nevertheless, from a fundamental standpoint, **Li_8IrO_6** ($4Li_2O{\cdot}IrO_2$) is of particular interest because IrO_2 is a metal, i.e., the band gap is zero; it therefore offers a unique opportunity to investigate the electronic behavior of the IrO_2 electrode as a function of Li_2O content. Moreover, IrO_2 and Pt/PtO_2 have been investigated as catalysts for the oxygen evolution reaction in fuel cells, photosynthesis,[49] water splitting[50], and Li-O_2 batteries.[51] A fundamental understanding of the effects of catalysis on the proposed hybrid Li-ion/Li-O_2 reaction may be obtained from studying these compounds and such insights will be valuable across different energy storage and conversion technologies involving oxygen.

Finally, the two metalloid oxides, **Li_6TeO_6** and **Li_5SbO_5,** are distinct because they offer high voltages, relative to the other reactions that pass this screen. The reactions are characterized by an uncommon combination of high-voltage and narrow band gap compounds. In the next section, we relax the screening criteria and show that the majority of

other high-voltage reactions occur at the cost of wider band gap materials.

3.2 Predictions - relaxed constraints

The reactions described in **Table 1** are those that meet all performance metrics, yet there are many other reactions that perform well in all but one metric. In Figure 7, fourteen reactions are highlighted that pass a new set of constraints, allowing for voltages up to 5 V and removing the band gap restriction entirely. The full reaction path and corresponding voltages, capacities and band gaps for these reactions are shown in **Table 2**. This second set of reactions is included in this screen because, while these criteria are not ideal, it may be possible to engineer solutions to overcome the limitations of these reactions. For example, the development of stable electrolytes may allow the use of high voltage materials thus rendering the voltage constraint unnecessary. Similarly, the problem of poor electronic conductivity may be alleviated by doping, nanosizing or dispersion of the electrode particles in a highly conducting matrix, as has been demonstrated for $LiFePO_4$ that has intrinsically poor electronic conductivity.[52, 53, 54, 55]

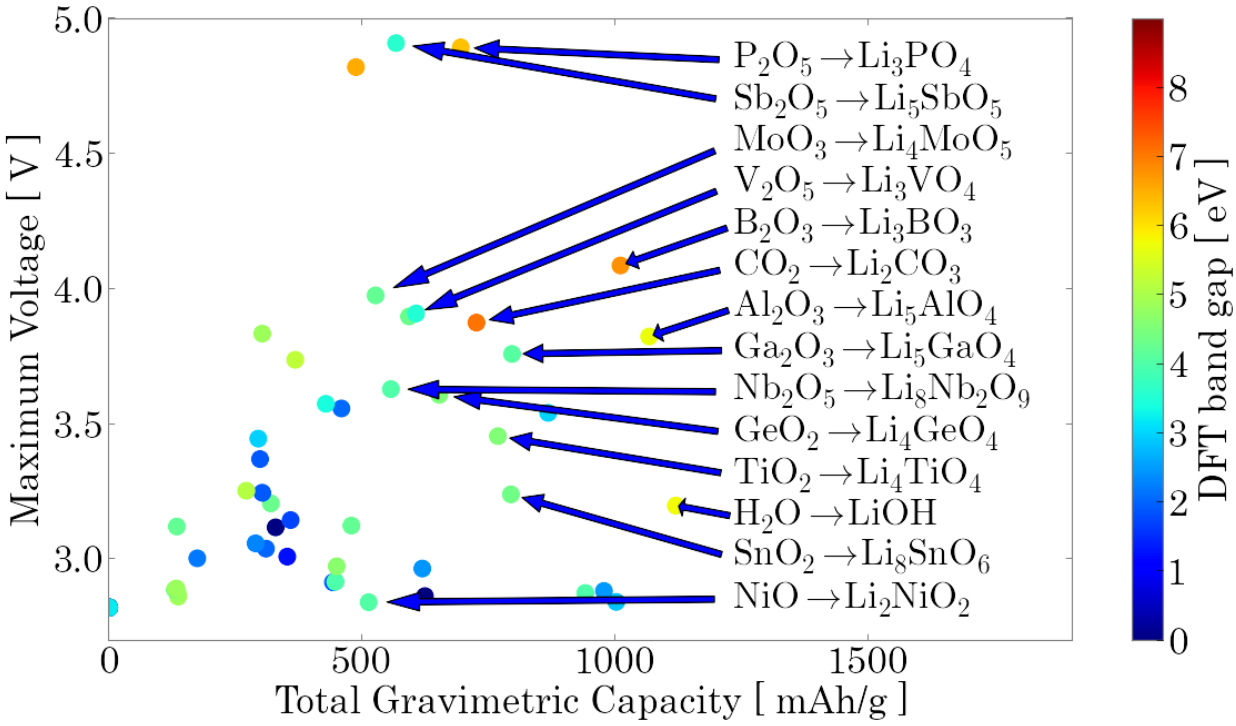

Figure 7. Relaxing the reaction criteria, i.e., increasing the cutoff voltage to 5.0 V and removing the band gap cutoff, results in 37 reactions that pass the screen. 14 reactions that provide more than 500 mAh/g capacity are identified by arrows.

Table 2. Full reaction pathway for each reaction which passes the relaxed screens. For each step the product phases, voltage, gravimetric and volumetric capacities, energy density and specific energy is reported.

Reaction steps	Voltage [V]	C_g [mAh/g]	C_V [mAh/mL]	E_g [Wh/kg]	E_V [Wh/L]	Bandgap [eV]
Li_2NiO_2						
→ NiO	2.8	513	2147	1447	6059	4.1
Li_4TiO_4						
→ Li_2TiO_3	2.9	384	998	1084	2818	4.6
→ TiO_2	3.5	768	1997	2208	5743	3.0
Li_3VO_4						
→ LiV_3O_8	3.7	526	1419	1486	4004	4.3
→ V_2O_5	4.2	592	1596	1731	4665	2.0
Li_4MoO_5						
→ Li_2MoO_4	3.0	263	1018	743	2873	2.6
→ MoO_3	4.0	526	2036	1521	5884	4.2
$Li_8Nb_2O_9$						
→ Li3NbO4	2.9	139	493	393	1392	3.4
→ LiNbO3	3.4	417	1480	1213	4300	4
→ Nb2O5	3.6	556	1973	1679	5953	3.5
Li_3BO_3						
→ $LiBO_2$	3.2	673	1483	1900	4184	5.6
→ $Li_2B_4O_7$	3.6	842	1853	2439	5371	6.0
→ LiB_3O_5	3.6	898	1977	2642	5817	7.1
→ B_2O_3	4.0	1010	2224	3048	6712	6.9
Li_8SiO_6						
→ Li_4SiO_4	2.8	597	1335	1684	3767	4.7

→	Li_2SiO_3	3.1	896	2003	2531	5662	5.2
→	$Li_2Si_2O_5$	3.5	1045	2336	2997	6704	5.5
→	$Li_2Si_3O_7$	3.5	1095	2448	3169	7088	5.4
→	SiO_2	3.5	1194	2670	3518	7869	5.6
Li_4GeO_4							
→	Li_2GeO_3	3.1	326	1039	920	2930	4.5
→	$Li_4Ge_5O_{12}$	3.6	522	1662	1527	4862	3.8
→	GeO_2	3.6	652	2077	1993	6346	3.2
Li_8SnO_6							
→	Li_2SnO_3	2.9	595	2036	1679	5747	4.4
→	SnO_2	3.2	793	2715	2247	7689	3.6
Li_5AlO_4							
→	$LiAlO_2$	2.9	853	1945	2407	5489	5.1
→	$LiAl_5O_8$	3.4	1023	2334	2899	6611	4.9
→	Al_2O_3	3.8	1066	2431	3044	6942	5.7
Li_5GaO_4							
→	$LiGaO_2$	2.9	637	1882	1796	5310	4.1
→	$LiGa_5O_8$	3.5	764	2258	2164	6397	3.5
→	Ga_2O_3	3.8	796	2352	2276	6728	3
Li_2CO_3							
→	CO_2	3.9	725	1557	2047	4393	5.2
Li_3PO_4							
→	$Li_4P_2O_7$	3.9	231	584	653	1648	6.3
→	$LiPO_3$	4.2	463	1167	1563	3943	6.2
→	P_2O_5	4.8	694	1751	2535	6394	6.0
LiOH							
→	LiH_3O_2 ($LiOH{\cdot}H_2O$)	3.1	746	1185	2105	3344	4.6
→	H_2O	3.2	1119	1778	3264	5184	5.3

Several classes of compounds and reactions that pass the relaxed criteria are identified: five transition metal oxides (**Li_2NiO_2**, **Li_4TiO_4**, **Li_3VO_4**, **Li_4MoO_5**, **$Li_8Nb_2O_9$**), three metalloid oxides (**Li_3BO_3**, **Li_8SiO_6**, **Li_4GeO_4**), three non-transition metal oxides (**Li_8SnO_6**, **Li_5AlO_4**, **Li_5GaO_4**), and three non-metal oxides (**Li_2CO_3**, **LiOH**, **Li_3PO_4**).

In this screen, the transition-metal oxidation state in **Li_2NiO_2**, **Li_4TiO_4**, **Li_4MoO_5**, **Li_3VO_4**, **$Li_8Nb_2O_9$** varies from a divalent state (Ni^{2+}) to a hexavalent state (Mo^{6+}). In general, the voltage increases across this spectrum of materials with oxidation state, from 2.8 V for Ni^{2+} to 4.2 V for V^{5+}. It is also found that the transition metal oxides have systematically lower band gaps relative to the non-transition metal oxides, metalloid oxides, and non-metal oxides. Because the voltage for the Li_2NiO_2 reaction is low, competition with Li_2O_2 formation during discharge is of concern. The Ti, Mo, and V systems do not suffer from this drawback. **Li_4TiO_4** is the only predicted material, besides Li_5FeO_4 and Li_6MnO_4, to have

been studied as an electrode in a non-aqueous Li-O_2 cell. In this respect, Lee *et. al.* have reported that a TiO_2 electrode, when operated in a non-aqueous electrolyte in the presence of oxygen, provided significantly higher capacity than in an inert nitrogen or argon environment.[56] This finding appears to be consistent with our predictions. **Li_3VO_4** is of interest as a fast Li^+-ion conductor[57] and, therefore, like Li_6ZnO_4, may be worth investigating to determine the reaction kinetics of lithium when used as an electrode in a Li-O_2 cell.

Next, the two non-transition-metal oxides are considered. **Li_8SnO_6** ($4Li_2O{\cdot}SnO_2$) is noteworthy because the SnO_x-Li_2O system has been exploited as an anode material for lithium-ion batteries. During the reaction with lithium, Sn is displaced from the SnO_x host structure to generate a matrix of Sn and Li_2O; thereafter, Li reacts reversibly and predominantly with Sn. However, by allowing the reaction of Li and SnO_2 to proceed in the presence of oxygen, our calculations show that the reaction may incorporate the oxygen to deliver a significantly higher capacity and voltage (3.2 V for the $SnO_2 \rightarrow Li_2SnO_3$ reaction) than SnO_x-Li_2O anodes in lithium-ion cells.[58] The second non-transition metal oxide, **Li_5AlO_4**, has the defect anti-fluorite structure of Li_5FeO_4. Because it is isostructural with Li_5FeO_4, it presents an opportunity to study the mixed-metal oxide solid solution system $Li_5Fe_{1-x}Al_xO_4$ which, like the Fe-Zn analog, has shown improved ion conductivity compared to either end compound.[48] It will be instructive to determine the influence that Al substitution would have on the electrochemical properties of Li_5FeO_4. The final non-transition metal oxide, **Li_5GaO_4,** is a close analogue to Li_5AlO_4, sharing the same reaction steps, with nearly identical voltages throughout. The striking difference between the Ga and Al compounds is the substantially smaller band-gaps among the Ga-containing compounds. These properties may be taken advantage of by doping Li_5AlO_4 with Ga in order to improve electronic conductivity without otherwise significantly affecting the thermodynamically stable reaction path.

The three metalloid oxides (**Li_3BO_3**, **Li_8SiO_6**, **Li_4GeO_4**) are all good Li-ion conductors,[59–61] but at the same time they are high band gap materials and operate at high voltage, thereby limiting their appeal as electrodes for Li-O_2 cells. Similar unfavorable trends are observed for the three non-metal oxides (**Li_2CO_3**, **LiOH, Li_3PO_4**). **LiOH** is the reaction product of a discharged, *aqueous* Li-O_2 cell.[62] It was only because no restrictions were imposed on elements during the screening process that we were we able to identify this reaction. This finding therefore highlights the power of materials screening without making *a priori* assumptions about the type of reactions under investigation. **Li_2CO_3** is predicted to decompose electrochemically during charge to produce CO_2 and O_2 (**Table 2**), at an attractive 3.9 V. However, although Li/CO_2 cells have been studied in their own right,[63] Li_2CO_3 cannot be readily decomposed in practice. This limitation and the difficulty in recombining lithium with two gasses during discharge makes Li_2CO_3 an unattractive candidate for rechargeable Li-O_2 cells.

3.3 Competition with oxidation/reduction

It has been assumed that all the reactions described above proceed by lithium removal and oxygen release. For transition metal oxides, in particular, the possibility exists that lithium extraction may also be accompanied by the oxidation of the transition metal ion. Table 3 lists the predicted voltages corresponding to the removal of lithium and oxygen, as well for lithium alone from the defect anti-fluorite structures Li_6FeO_4, Li_6CoO_4 and Li_6MnO_4.

Table 3. Comparison of voltages for the first Li/O removal step with the removal of a single Li atom (labeled 1st Li).

Composition	Li/O [V]	1st Li [V]
Li_5FeO_4	2.9	3.85
Li_6CoO_4	2.9	2.36
Li_6MnO_4	2.9	2.38

The voltage to remove a *single* Li atom was determined by removing lithium from

each of the symmetrically distinct lithium sites, and completely relaxing the structure within DFT. Based on these Li vacancy formation energies, the lowest energy defect is used to compute the voltage for removing one Li atom,

$$V = (E_{Li_{y-1}MO_x} - E_{Li_yMO_x}) + \mu_{Li} \quad (8)$$

In Eq. 8, $E_{Liy-\delta MOx}$ is the energy of the perfect lithium metal oxide crystal, E_{LiyMOx} is the energy of the same crystal with a single lithium atom removed. For both Li_6MnO_4 and Li_6CoO_4, it is predicted that lithium alone would be removed at 2.38 and 2.36 V, respectively (Table 3), whereas the removal of both lithium and oxygen would occur at a higher potential, 2.9 V, for both materials. Therefore, it would be expected that for these two materials the electrochemical reaction would occur first by lithium removal alone. In contrast, for Li_5FeO_4, lithium extraction is predicted to occur at 3.85 V, i.e., significantly higher than the energetically more favored removal of both lithium and oxygen at 2.9 V. The mechanisms by which lithium and oxygen are electrochemically removed from Li_5FeO_4 and re-accommodated by the charged product are not yet understood and require further study. Likewise, detailed studies of the reversibility and structural changes during electrochemical cycling for the various materials found in the screen are essential before they can be applied in practical batteries.

4. Conclusions

A wide range of battery chemistries for Li-O_2 cells that involve the removal of lithium and oxygen from a parent host structure, analogous to the reaction that occurs with Li_5FeO_4, has been explored using a large thermochemical database. The search was implemented using DFT to determine the ground state thermodynamics of every system which could react in this manner. For every reaction, the voltage, gravimetric and volumetric charge capacity, as well as energy density and specific energy, was computed. New reactions were screened using a 4-step process to constrain the search to composition, thermodynamics (reaction pathway),

kinetics (electrolyte stability and electrical conductivity), and capacity. To approximate the electronic conductivity of each compound, the DFT band gap was used. Based on these metrics, 22 possible materials and reactions with a capacity exceeding 500 mAh/g were identified. The screening process was validated by identifying a few reactions that have already been explored in Li-O_2 cells, notably LiOH, Li_4TiO_4 and Li_5FeO_4. From an initial pool of many thousand candidate materials, computational screening revealed 22 materials of potential interest, four of which were identified as being worthy of further study, notably, Li_6CoO_4 ($3Li_2O{\cdot}CoO$), Li_6MnO_4 ($3Li_2O{\cdot}MnO$) and Li_4MoO_5 ($2Li_2O{\cdot}MoO_3$) and Li_8IrO_6.

Acknowledgements

This work was supported by the Center for Electrical Energy Storage: Tailored Interfaces, an Energy Frontier Research Center funded by the U.S. Department of Energy, Office of Science, Office of Basic Energy Sciences. Use of the Center for Nanoscale Materials was supported by the U. S. Department of Energy, Office of Science, Office of Basic Energy Sciences, under Contract No. DE-AC02-06CH11357. This research used resources of the National Energy Research Scientific Computing Center, which is supported by the Office of Science of the U.S. Department of Energy under Contract No. DE-AC02-05CH11231. The authors would like to acknowledge Alper Kinaci for helpful discussions and comments.

References

1. M. M. Thackeray, C. Wolverton, and E. D. Isaacs, *Energy Environ. Sci.*, 2012, **5**, 7854–7863.
2. B. Scrosati, J. Hassoun, and Y. Sun, *Energy Environ. Sci.*, 2011, **4**, 3287–3295.
3. P. G. Bruce, L. J. Hardwick, and K. M. Abraham, *MRS Bull*, 2011, **36**, 506–512.
4. N. Garcia-Araez and P. Novák, *J. Solid State Electrochem.*, 2013, **17**, 1793–1807.

5. M. Park, H. Sun, H. Lee, J. Lee, and J. Cho, *Adv. Energy Mater.*, 2012, **2**, 780–800.

6. J. Lee, S. T. Kim, R. Cao, N.-S. Choi, M. Liu, K. T. Lee, and J. Cho, *Adv. Energy Mater.*, 2011, **1**, 34–50.

7. A. Kraytsberg and Y. Ein-Eli, *J. Power Sources*, 2010, **196**, 886–893.

8. G. Girishkumar, B. McCloskey, a. C. Luntz, S. Swanson, and W. Wilcke, *J. Phys. Chem. Lett.*, 2010, **1**, 2193–2203.

9. J. Christensen, P. Albertus, R. S. Sanchez-Carrera, T. Lohmann, B. Kozinsky, R. Liedtke, J. Ahmed, and A. Kojic, *J. Electrochem. Soc.*, 2012, **159**, R1.

10. K. G. Gallagher, S. Goebel, T. Greszler, M. Mathias, W. Oelerich, D. Eroglu, and V. Srinivasan, *Energy Environ. Sci.*, 2014.

11. Y. Shao, S. Park, J. Xiao, J. Zhang, Y. Wang, and J. Liu, *ACS Catal.*, 2012, **2**, 844–857.

12. L. Trahey, C. Johnson, J. Vaughey, S.-H. Kang, L. J. Hardwick, S. A. Freunberger, P. G. Bruce, and M. M. Thackeray, *Electrochem. Solid-State Lett.*, 2011, **14**, A64.

13. L. Trahey, N. K. Karan, M. K. Y. Chan, J. Lu, Y. Ren, J. Greeley, M. Balasubramanian, A. K. Burrell, L. A. Curtiss, and M. M. Thackeray, *Adv. Energy Mater.*, 2013, **3**, 75–84.

14. M. M. Thackeray, M. K. Y. M. Chan, L. Trahey, S. Kirklin, and C. Wolverton, *J. Phys. Chem. Lett.*, 2013, **4**, 3607–3611.

15. C. S. Johnson, S.-H. Kang, J. T. Vaughey, S. V. Pol, M. Balasubramanian, and M. M. Thackeray, *Chem. Mater.*, 2010, **22**, 1263–1270.

16. A. Belsky, M. Hellenbrandt, V. L. Karen, and P. Luksch, *Acta Crystallogr. Sect. B*, 2002, **58**, 364–369.

17. A. R. Akbarzadeh, V. Ozoliņš, and C. Wolverton, *Adv. Mater.*, 2007, **19**, 3233–3239.

18. C. Wolverton, D. J. Siegel, A. Akbarzadeh, and V. Ozoliņš, *J. Phys. Condens. Matter*, 2008, **20**, 064228.

19. J. Saal, S. Kirklin, M. Aykol, B. Meredig, and C. Wolverton, *JOM*, 2013, **65**, 1501–1509.

20. G. Ceder, *Comput. Mater. Sci.*, 1997, **8**, 161–169.

21. G. Ceder, Y. M. Chiang, and D. R. Sadoway, *Nature*, 1998, **392**, 694–696.

22. S. Kirklin, B. Meredig, and C. Wolverton, *Adv. Energy Mater.*, 2013, **3**, 252–262.

23. G. Ceder, *MRS Bull.*, 2010, **35**, 693–702.

24. P. Hohenberg and W. Kohn, *Phys. Rev.*, 1964, **136**, 864–871.

25. W. Kohn and L. J. Sham, *Phys. Rev.*, 1965, **140**, 1133–1138.

26. G. Kresse and J. Hafner, *Phys. Rev. B*, 1993, **47**, 558–561.

27. G. Kresse and J. Hafner, *Phys. Rev. B*, 1994, **49**, 14251–14269.

28. G. Kresse and J. Furthmüller, *Phys. Rev. B*, 1996, **54**, 11169–11186.

29. G. Kresse and J. Furthmuller, *Comput. Mater. Sci.*, 1996, **6**, 15–50.

30. P. E. Blöchl, *Phys. Rev. B*, 1994, **50**, 17953–17979.

31. J. P. J. Perdew, K. Burke, and M. Ernzerhof, *Phys. Rev. Lett.*, 1996, **77**, 3865–3868.

32. G. Kresse and D. Joubert, *Phys. Rev. B*, 1999, **59**, 1758–1775.

33. L. Wang, T. Maxisch, and G. Ceder, *Phys. Rev. B*, 2006, **73**, 195107.

34. S. Grindy, B. Meredig, S. Kirklin, J. E. Saal, and C. Wolverton, *Phys. Rev. B*, 2013, **87**, 075150.

35. SGTE, *Thermodynamic properties of inorganic materials, vol. 19*, Springer-Verlag, Berlin, Heidelberg, 1999.

36. V. Stevanović, S. Lany, X. Zhang, and A. Zunger, *Phys. Rev. B*, 2012, **85**, 115104.

37. C. Barber, D. Dobkin, and H. Huhdanpaa, *ACM Trans. Math. Softw.*, 1996, **22**, 469–483.

38. B. Scrosati, *Electrochim. Acta*, 2000, **45**, 2461–2466.

39. Z. Zhang, L. Hu, H. Wu, W. Weng, M. Koh, P. C. Redfern, L. A. Curtiss, and K. Amine, *Energy Environ. Sci.*, 2013, 1806–1810.

40. J. Hummelshøj, J. Blomqvist, S. Datta, T. Vegge, J. Rossmeisl, K. S. Thygesen, A. C. Luntz, K. W. Jacobsen, and J. K. Norskov, *J. Chem. Phys.*, 2010, **132**, 071101.

41. L. Sham and M. Schlüter, *Phys. Rev. Lett.*, 1983, **51**, 1888–1891.

42. J. Perdew and M. Levy, *Phys. Rev. Lett.*, 1983, **51**, 1884–1887.

43. J. Perdew, *Int. J. Quantum Chem. Quantum Chem. Symp.*, 1985, **19**, 497–523.

44. M. Chan and G. Ceder, *Phys. Rev. Lett.*, 2010, **105**, 196403–196407.

45. L. Liang, J. Luo, M. Chen, L. Wang, L. Jianjun, and H. Xiangming, *Int. J. Electrochem. Soc.*, 2013, **8**, 6393–6398.

46. S. Narukawa, Y. Takeda, M. Nishijima, N. Imanishi, O. Yamamoto, and M. Tabuchi, *Solid State Ionics*, 1999, **122**, 59–64.

47. I. Raistrick, C. Ho, and R. Huggins, *Mater. Res. Bull.*, 1976, **II**, 953–957.

48. T. Esaka and M. Greenblatt, *J. Solid State Chem.*, 1987, **71**, 164–171.

49. R. Ramaraj and M. Kaneko, *Curr. Sci.*, 1994, **66**, 735–741.

50. V. K. Puthiyapura, S. Pasupathi, H. Su, X. Liu, B. Pollet, and K. Scott, *Int. J. Hydrogen Energy*, 2014, **39**, 1905–1913.

51. Y.-C. Lu, Z. Xu, H. a Gasteiger, S. Chen, K. Hamad-Schifferli, and Y. Shao-Horn, *J. Am. Chem. Soc.*, 2010, **132**, 12170–1.

52. A. K. Padhi, K. S. Nanjundaswamy, and J. B. Goodenough, *J. Electrochem. Soc.*, 1997, **144**.

53. S.-Y. Chung, J. T. Bloking, and Y.-M. Chiang, *Nat. Mater.*, 2002, **1**, 123–8.

54. H. Huang, S.-C. Yin, and L. F. Nazar, *Electrochem. Solid-State Lett.*, 2001, **4**, A170.

55. B. Kang and G. Ceder, *Nature*, 2009, **458**, 190–3.

56. B. Lee, S. Nam, and J. Choi, *Curr. Appl. Phys.*, 2012, **12**, 1580–1585.

57. J. Kuwano and A. R. West, *Mater. Res. Bull.*, 1980, **15**, 1661–1667.

58. Y. Idota, T. Kubota, A. Matsufuji, Y. Maekawa, and T. Miyasaka, *Science*, 1997, **276**, 1395–1397.

59. S. Ohta, S. Komagata, J. Seki, T. Saeki, S. Morishita, and T. Asaoka, *J. Power Sources*, 2013, **238**, 53–56.

60. A. Robertson and A. R. West, *Solid State Ionics*, 1992, **58**, 351–358.

61. A. Khorassani and A. R. West, *Solid State Ionics*, 1982, **7**, 1–8.

62. W. Li, J. R. Dahn, and D. S. Wainwright, *Science*, 1994, **264**, 1115–8.

63. K. Takechi, T. Shiga, and T. Asaoka, *Chem. Commun.*, 2011, **47**, 3463–5.